THE JOURNAL OF PHYSICAL CHEMISTRY C

Article

pubs.acs.org/JPCC

Local Characterization of Ultrathin ZnO Layers on Ag(111) by Scanning Tunneling Microscopy and Atomic Force Microscopy

Akitoshi Shiotari,[†,§] Bo Hong Liu,[‡] Simon Jaekel,[†,∥] Leonhard Grill,[†,∥] Shamil Shaikhutdinov,[‡] Hans-Joachim Freund,[‡] Martin Wolf,[†] and Takashi Kumagai*[,†]

[†]Department of Physical Chemistry and [‡]Department of Chemical Physics, Fritz-Haber Institute of the Max-Planck Society, Faradayweg 4-6, 14195 Berlin, Germany

[§]Department of Chemistry, Graduate School of Science, Kyoto University, Kitashirakawa-Oiwake-cho, 606-8502 Kyoto, Japan

[∥]Department of Physical Chemistry, University of Graz, Heinrichstrasse 28, 8010 Graz, Austria

Supporting Information

ABSTRACT: We have studied the local structure of ultrathin ZnO layers grown on Ag(111) by the reactive deposition method using low-temperature scanning tunneling microscopy (STM) and noncontact atomic force microscopy (nc-AFM) at 5 K. The characteristic Moiré patterns arising from the lattice mismatch between the ZnO(0001) layers and Ag(111) appear in STM, but it is not pronounced in nc-AFM images. This indicates an atomically flat geometrical structure of the ZnO layer and a dominant contribution of the electronic state to the Moiré patterns imaged by STM. We found that the apparent height of STM for the ZnO layers strongly depends on the bias voltage and becomes comparable with that of nc-AFM when the bias voltage is below the conduction band edge of the ZnO layers. The ZnO layers with the STM (AFM) apparent height of 3.8 (4.0) ± 0.3 and 5.8 (6.1) ± 0.3 Å were observed. On the other hand, mapping the onset of the resonance state of the ZnO layer by scanning tunneling spectroscopy provides a basis for determining its thickness. Our results suggest that the ZnO layers on Ag(111) grow predominantly as bi- and trilayers under the conditions used.

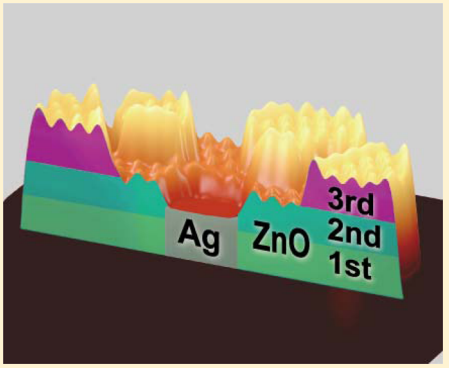

INTRODUCTION

Ultrathin oxide films grown on single-crystalline metal supports, which have a well-defined structure, have been employed as model systems to investigate the elementary processes in heterogeneous catalysis at the atomic scale.[1−3] Previous studies revealed that the geometric and electronic structure[4−9] and catalytic properties[10,11] of ultrathin (a few monolayers thick) oxide films may be different from those of thicker films or the bulk oxide. For instance, a significant enhancement of the CO oxidation rate was observed for a monolayer thick iron oxide film on Pt(111) compared to the bare Pt surface and nm thick films.[10] In principle, the film thickness may influence the catalytic activity due to the different structural and electronic properties. In addition, for a film partially covering metal surfaces the catalytic effect may originate from the oxide/metal interface and as such depend on the metal support. The catalytic effect is often attributed to the existence of (local) active sites. For instance, the CO oxidation rate for the ZnO films on Pt(111) at a near atmospheric pressure and relatively low temperature (450 K) shows the maximum at about 70% coverage,[12] indicating that edges of the oxide film play a crucial role in the process. On the other hand, the CO oxidation is inhibited when ZnO films are grown on Ag(111).[13] Therefore, the local structural and electronic properties are of fundamental importance for a comprehensive understanding of the catalytic effect in ultrathin oxide materials. In addition, such a local structure of ultrathin oxide films is closely related with the microscopic growth mechanism. The scanning tunneling microscope (STM) has been a powerful tool to investigate the local surface morphology (structure), electronic property, and growth behavior of oxide films at the atomic scale.[8]

ZnO-based systems represent an important class of the catalysts for the water-gas shift reaction and methanol synthesis.[14−16] ZnO is also emerging as a prominent material for optoelectronic applications, i.e., photovoltaics, light-emitting devices, laser diode, and photodetectors,[17,18] because of its wide optical band gap (3.4 eV), low cost, and ease of fabrication. The gap can be tuned by doping with various cations and anions.[19] However, the detailed characterization of the bulk surface has often been hampered by the existence of unknown dopants and defects. In this context, it is of fundamental interest to understand the surface structures and local physical/chemical properties of ZnO.

In this work we study ultrathin ZnO layers grown on Ag(111). The formation of ZnO overlayers on low index silver

Received: September 5, 2014
Revised: October 15, 2014
Published: November 4, 2014

dx.doi.org/10.1021/jp509013p | J. Phys. Chem. C 2014, 118, 27428−27435

surfaces was first studied by Kourouklis and Nix.[20] They investigated the growth of the ZnO layers via the oxidation of a Zn thin film on silver surfaces by Auger electron spectroscopy (AES). Their low-energy electron diffraction (LEED) analysis revealed that the film prepared at 300 K shows no long-range order. However, upon heating to about 500 K ordered domains appeared with a structure similar to ZnO(0001). ZnO(0001) is a polar surface with a finite dipole moment perpendicular to the surface (Tasker type III), but the reconstruction to a nonpolar graphitic hexagonal structure has recently been predicted for free-standing films.[21,22] Shortly after, using a combination of surface X-ray diffraction (SXRD) and STM, Tusche et al.[23] reported atomically flat ZnO(0001) films on Ag(111) and a transition from a relaxed graphitic hexagonal structure for 2 ML to a bulk-like wurtzite structure at the film thickness of 3 or 4 monolayers. It was also found that the ultrathin ZnO films on Ag(111) exhibit a Moiré pattern in the STM image due to a lattice mismatch with the Ag(111) substrate. The ZnO film was formed by pulsed laser deposition on Ag(111) at 300 K under an oxygen background pressure of 5×10^{-7} mbar and subsequent annealing to 680 K. To deposit ZnO onto Au(111), Stavale et al.[24] evaporated ZnO pellets in 5×10^{-5} mbar of O_2 followed by annealing at 600−800 K. They observed mono- and multilayer ZnO layers with STM and measured luminescence spectra for the multilayer layers. Pan et al.[13] employed the reactive deposition method to grow the ZnO layers on Ag(111) and Cu(111) whereby Zn is deposited onto the substrate at room temperature in 10^{-5} mbar of O_2 followed by annealing up to 600 K under ultrahigh vacuum (UHV) conditions. Their LEED, AES, and STM results suggest primary growth of a bilayer ZnO(0001) on Ag(111). Moreover, Deng et al.[25] reported the growth of stoichiometric ZnO layers on Au(111) and showed that the bilayer is thermodynamically stable due to the stronger interfacial interaction between ZnO layers as compared to the interaction between a ZnO layer and Au(111) surface. They also used the reactive deposition method to grow the film on Au(111) but with the presence of NO_2 background pressure. For the reactive deposition method the background atmosphere may play a critical role in determining the film morphology (structure). Weirum et al.[26] studied the growth of ZnO films with a few monolayers thick on Pd(111) and found that the structure and thickness of ZnO islands depend on the oxygen pressure during the reactive deposition. On the basis of DFT calculations, they claimed that the nonpolar graphitic Zn_6O_6 structure is thermodynamically stable up to 4 ML over a wide range of oxygen chemical potentials. Schott et al.[27] recently reported an alternative approach to grow ZnO films using brass substrates, resulting in disordered ZnO films. In all these previous studies the thickness of ZnO layers was deduced by measuring the apparent height in STM. However, this is not straightforward because the apparent height in STM may strongly depend on the bias voltage. In particular, this will be complicated at the boundary between the bare metal and ultrathin metal oxide film because of their different electronic structure. For instance, the apparent height of ∼2.0 (4.0) Å was assigned to the characteristic height between the bare metal surfaces and monolayer (bilayer) thick ZnO(0001) on Pt(111)[12] and Pd(111).[26] However, Deng et al.[25] assigned ∼3.5 Å to monolayer ZnO(0001) on Au(111).

Here we investigate the local structure of ultrathin ZnO layers grown on Ag(111) using a simultaneous measurement of low-temperature (5 K) STM and noncontact atomic force microscopy (nc-AFM). The layer is grown by the reactive deposition method reported by Pan et al.[13] The characteristic Moiré pattern of ZnO layers is observed in STM, being in good agreement with previous reports,[23] but is not observed in nc-AFM, indicating an atomically flat geometrical structure of the ZnO layer. The apparent height in STM strongly depends on the bias voltage but becomes comparable with that obtained by nc-AFM when the bias voltage in STM is below the band gap of the ZnO layer. Our results suggest that bi- and trilayers is grown predominantly under the conditions used.

EXPERIMENTAL METHODS

The experiments were performed in an UHV chamber (base pressure of $\sim 2 \times 10^{-10}$ mbar) equipped with Omicron low-temperature STM/AFM utilizing a tuning fork sensor (qPlus sensor).[28,29] An etched tungsten tip was glued at the end of the oscillating prong in the tuning fork. The tuning fork is mechanically excited along the tip axis with a separated slice of piezo that is mounted on top of the z-piezo. The sensor used in the experiment had a resonance at ∼26 645 Hz with the quality factor of 20 000−40 000 at 5 K. We used the oscillation amplitude (A_{osc}) less than 1.5 nm for nc-AFM imaging. The bias voltage is applied either to the sample or tip denoting V_s and V_t, respectively, and all voltages are shown as V_s ($= -V_t$). For AFM measurements, in order to minimize possible crosstalk problems between the measured tunneling current I_t (STM) and the frequency shift Δf (AFM), the tunneling current is collected from the sample with carefully designed wiring (the frequency shift is read out from the tuning fork).[30] Scanning tunneling spectroscopy (STS) was recorded using a lock-in amplifier with a modulation of 12−30 mV_{rms} at 710 Hz. The STM/AFM measurements were performed at 5 K.

The Ag(111) surface was cleaned by repeated cycles of argon ion sputtering and annealing up to 670 K. The growth of ZnO layers on Ag(111) was achieved by the reactive deposition in a separated preparation chamber (base pressure of $< 5 \times 10^{-10}$ mbar), whereby Zn was evaporated onto Ag(111) at room temperature in the presence of O_2 (1×10^{-5} mbar) followed by annealing at 670 K under UHV conditions.[13] The rate of the temperature increase (decrease) was ∼0.7 (∼0.3) K/s. A relatively high O_2 partial pressure during Zn deposition was used to avoid possible alloying between Zn and Ag since the oxygen might suppress intermixing. Zn was evaporated by heating a Zn rod (1 mm in diameter, 99.9997% purity, from Alfa Aesar) in a Knudsen cell at a temperature of 480−490 K. The Zn source was placed at a distance of ∼15 cm from the Ag(111) surface and Zn was deposited through a small orifice (∼5 mm in diameter) attached to the cell. The heating temperature was read by a Type K thermocouple spot-welded to the bottom of the cell.

In addition, complementary studies on the film growth were performed in another UHV chamber equipped with an STM, AES, and LEED all operated at room temperature. Zn was deposited by heating a Zn rod (1 mm in diameter, 99.99% purity, from Goodfellow) to 480−520 K, passing current through a thoriated tungsten wire wrapped around the rod. The Zn source is shielded by a metal cylinder having a small orifice (∼5 mm in diameter) and placed about 2 cm away from a crystal. The deposition flux was controlled via a Type K thermocouple spot-welded to the edge of the Zn rod.

Note that due to differences in sample assembly and geometry of thermocouple connection, there may be some deviations in temperature reading (∼10 K) in these two setups.

dx.doi.org/10.1021/jp509013p | J. Phys. Chem. C 2014, 118, 27428−27435

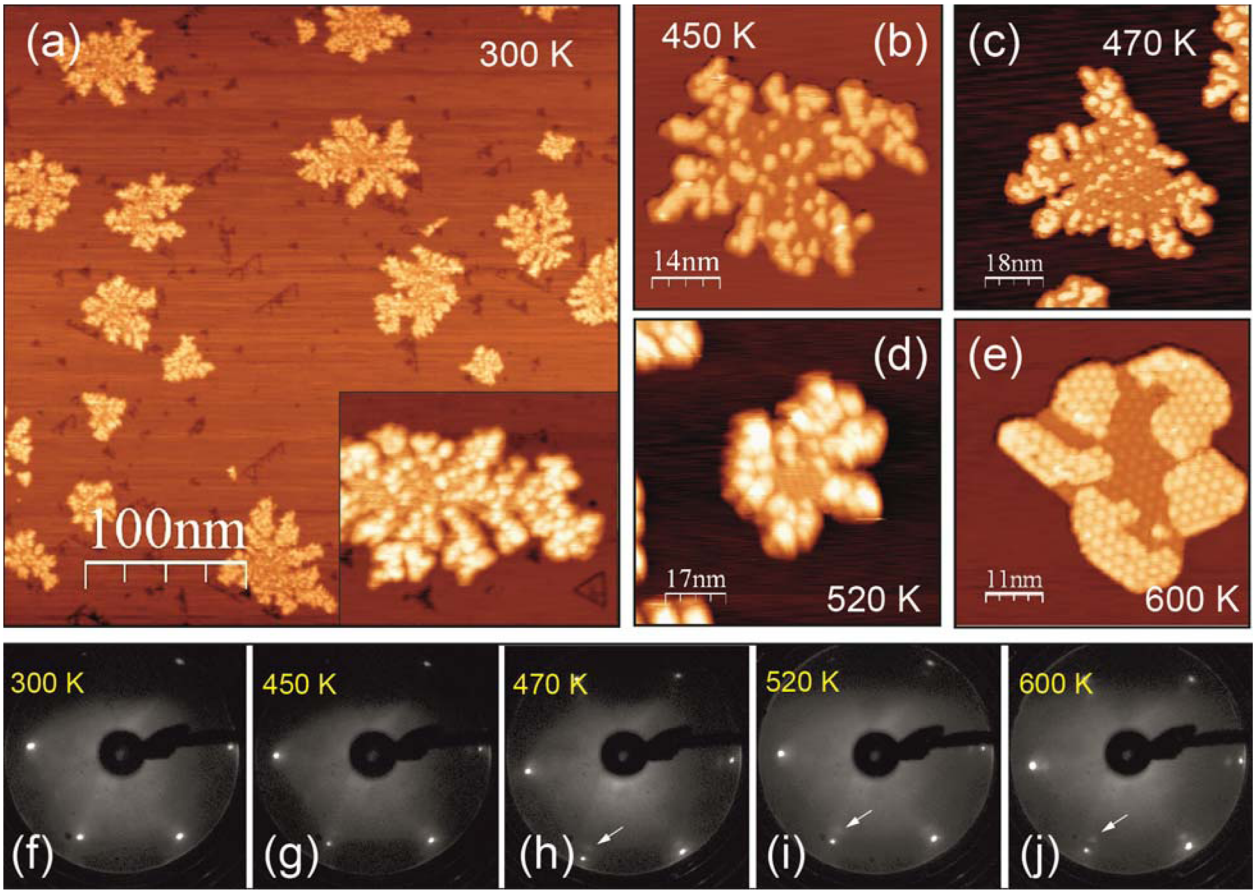

Figure 1. (a–e) STM images of the Ag(111) surface (a) upon reactive Zn deposition at 300 K (V_s = 1.2 V, I_t = 1.2 nA) and subsequent stepwise annealing in UHV at (b) 450 (V_s = 1.5 V, I_t = 0.4 nA), (c) 470 (V_s = 1.2 V, I_t = 0.8 nA), (d) 520 (V_s = 1.2 V, I_t = 0.8 nA), and (e) 600 K (V_s = 1.5 V, I_t = 1.0 nA) for 10 min. The images were obtained at room temperature. (f–j) The corresponding LEED patterns with the annealing temperature indicated. The arrows in (h–j) highlight progressive sharpening of the diffraction spots assigned to ZnO(0001) islands.

However, comparative STM studies showed the same behavior for morphology of ZnO deposits in both UHV chambers.

RESULTS AND DISCUSSION

Figure 1a shows a typical large-scale STM image of the Ag(111) surface prepared by Zn reactive deposition at 300 K at submonolayer coverage (no postannealing process). The image was obtained at room temperature. Dendritic structures (in the inset) are observed, which are indicative for diffusion-limited growth at these low temperatures. The lack of ordering structure is also confirmed by the corresponding LEED pattern only showing sharp diffraction spots from the Ag(111) surface (Figure 1f). In addition, some depressed pits and lines running in the main crystallographic directions of Ag(111) are imaged in Figure 1a. Their origin remains unclear, but they disappeared upon annealing, and cleanness of the bare Ag(111) surface was confirmed by its characteristic electronic surface state in STS. Therefore, they will not be discussed here. STM images and corresponding LEED patterns obtained after stepwise heating in UHV to 450 K (Figures 1b,g), 470 K (Figures 1c,h), and 520 K (Figures 1d,i) slightly improve long-range ordering (the additional diffraction spot appears in LEED as marked by arrows in Figure 1h). The islands become well-ordered and better shaped upon heating to above 600 K (Figures 1e,j). Annealing to higher temperatures leads to partial sublimation of ZnO.

As seen in Figure 1e, the well-ordered islands show a Moiré structure commonly assigned to the lattice mismatch between Ag(111) and ZnO(0001),[13,23] which is served as a fingerprint for the ZnO layers. The Moiré structure can be seen on both the low and high terraces of the ZnO island (Figures 1e). Interestingly, there are different Moiré structures, which are rotated with respect to each other and hence showing different periodicity (see details below). The high-ZnO layers in Figure 1e are dominantly observed at the edges of the ZnO islands. This suggests that the edges are local potential minima for the ZnO–ZnO interlayer interaction and that initial ZnO clusters on the low-ZnO layers (Figures 1b–d) diffused to the edges and aggregated to yield flat layers during the postannealing process.

Basically the same picture is observed for ZnO overlayers at high coverages. Figure 2a shows a typical STM image at ~60% coverage of ZnO layers, obtained at 5 K, where the remaining area consists of bare Ag terraces identified by their hexagonal structure in atomic resolution images with interatomic distances of a_{Ag} = 2.89 Å (not shown here) and the surface state in STS. The film edges are straight and follow preferential directions, which is characteristic for the ordered growth on a crystalline lattice. The inset of Figure 2a shows an STM image of a characteristic ZnO island with a central bare Ag patch. The apparent height of the Ag patch relative to the outside Ag terrace is ~2.4 Å, equal to the monatomic step height. Although a clean Ag(111) surface has almost straight step edges and

dx.doi.org/10.1021/jp509013p | J. Phys. Chem. C 2014, 118, 27428–27435

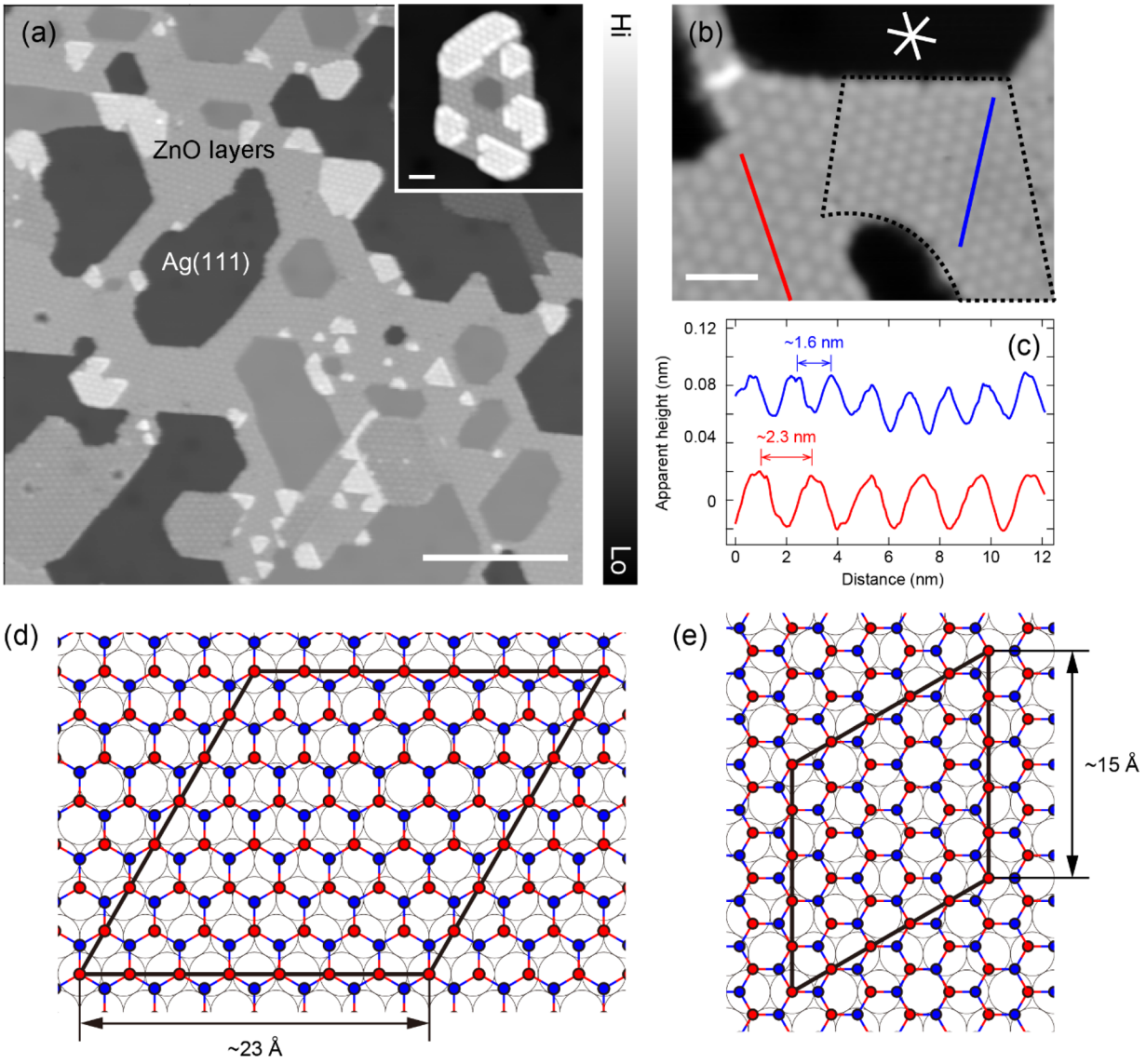

Figure 2. (a) STM overview image of ultrathin ZnO layers on Ag(111) (V_s = 1 V, I_t = 0.1 nA, scale bar = 50 nm) at 5 K, revealing both bare Ag(111) areas and ZnO layers. The sample was annealed up to 670 K after the reactive deposition, and the image was obtained at 5 K. The inset shows an STM image of a small ZnO island on the Ag(111) terrace (V_s = 1 V, I_t = 1 nA, scale bar = 5 nm). (b) Enlarged STM image (V_s = 1 V, I_t = 0.05 nA, scale bar = 5 nm) of the low-ZnO layer that shows the characteristic Moiré pattern aligned along the high-symmetry axes of Ag(111) (close-packed directions of the Ag(111) surface are marked by the three white lines in the upper part). The framed area (back dashed line) highlights the misaligned area. (c) Line profiles for the aligned (red) and misaligned (blue) Moiré area (indicated in Figure 1b). The latter profile is vertically offset for clarity. (d, e) Schematic illustrations of (d) ZnO(0001)-(7 × 7)/Ag(111)-(8 × 8) and (e) ZnO(0001)-(5 × 5)/Ag(111)-($3\sqrt{3}$ × $3\sqrt{3}$) $R30°$ coincidence structures. The unit cell of the Moiré pattern is indicated by black lines. Blue, red, and gray circles represent Zn, O, and Ag atoms, respectively.

exhibits no small Ag patches, they are modified and form a zigzag edge of ZnO layers (Figure 2a). Similar modifications of metal surfaces have been reported for ZnO/Cu(111),[13] cobalt oxide films on Ag(001),[31] and nickel oxide on Ag(001).[32,33] This implies that Ag atoms diffuse and reconstruct the surface along with the growth of ZnO films, leading to formation of characteristic structures like Ag patches. Figure 2b shows an enlarged STM image of the low-ZnO layer. As shown by the red line in Figure 2b, the Moiré pattern is predominantly aligned along the high-symmetry atomic row direction of Ag(111) (indicated as the three white lines in the upper part of Figure 2b). A line profile measured along the red line (the red curve in Figure 2c) indicates that the Moiré structure exhibits a periodicity of ~23 Å, corresponding to the ZnO(0001)-(7 × 7)/Ag(111)-(8 × 8) coincidence structure (Figure 1d), as reported previously.[13,23] The lattice constant of the ZnO films ($a_{ZnO,film}$ = 3.30 Å) is strained by ~2% relative to the bulk ZnO(0001) lattice ($a_{ZnO,bulk}$ = 3.25 Å). In addition, we also observed a "misaligned" Moiré structure with different azimuthal orientations up to 30° relative to the Ag atomic row (high-symmetry direction). A similar observation has been reported for boron nitride monolayers on Cu(111), where different Moiré-phase domains have been observed. The rotated Moiré area by 30° is indicated by the black dashed line in Figure b, where the periodicity of ~16 Å is observed (the blue curve in Figure 2c). This is approximately equal to $3\sqrt{3}\,a_{Ag}$ (~15 Å), suggesting ZnO(0001)-(5 × 5)/Ag(111)-

dx.doi.org/10.1021/jp509013p | J. Phys. Chem. C 2014, 118, 27428−27435

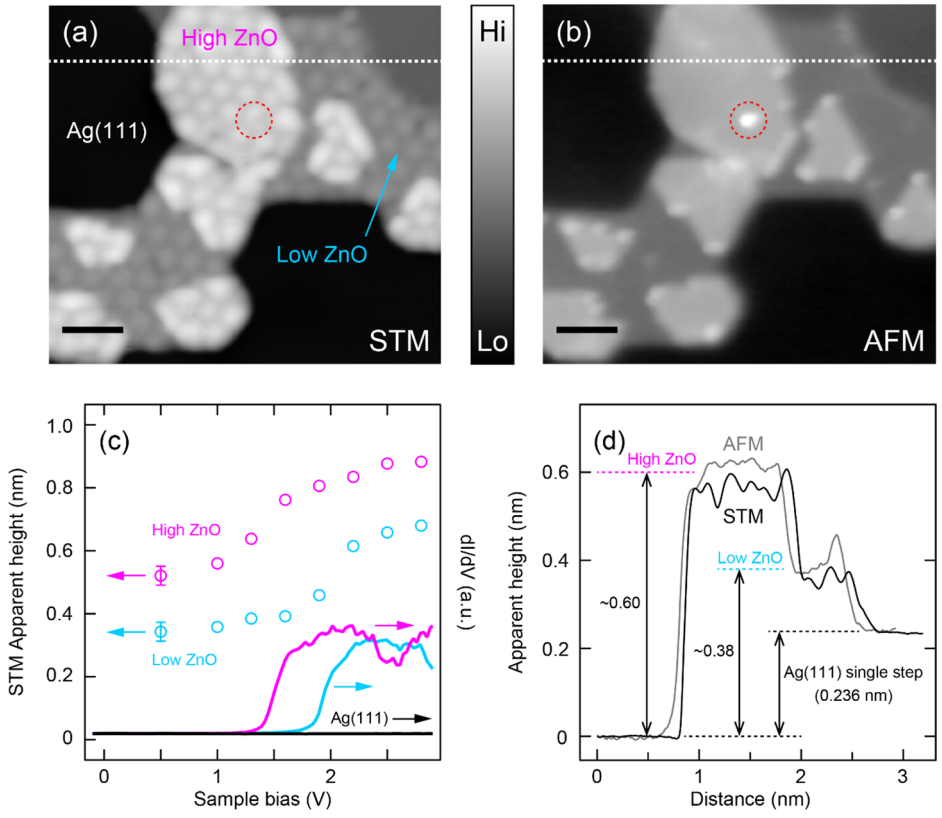

Figure 3. (a, b) STM image (V_s = 1 V, I_t = 1 nA) and nc-AFM image (V_s = 0 V, Δf = −1 Hz, A_{osc} = 1.5 nm) obtained at the same area (scale bar = 5 nm) at 5 K. The dotted circle represents a defect on the high-ZnO island. (c) Voltage dependence of the STM apparent height (left axis) and dI/dV spectra (right axis) measured for the bare Ag surface (black) and the low-ZnO (cyan) and high-ZnO (red) layers. (d) Line profiles for the STM (black curve) and nc-AFM (gray curve), indicated by the white dashed line in (a) and (b), respectively.

$(3\sqrt{3} \times 3\sqrt{3})$ $R30°$ structure as a possible structure. The corresponding lattice constant of the ZnO layer is 3.00 Å, and therefore, the lattice is contracted by ∼8% relative to $a_{ZnO,bulk}$. This suggests that the misaligned structure is less stable and forms much smaller domains than the dominant ZnO-(7 × 7)/Ag-(8 × 8) structure (Figure 1e). The existence of several domains with slightly different azimuthal orientations was observed in large-scale STM images, which is corroborated by streaky ZnO-related diffraction spots in corresponding LEED patterns (see the Supporting Information). Such streaky LEED spots have also been observed for ZnO films on Pt(111).[12]

In order to investigate the structure of the low- and high-ZnO layers, we performed simultaneous STM and nc-AFM imaging. The tuning fork (qPlus) sensor makes it possible to record both channels and the tip position (relative distance between the tip and surface) can be controlled via either of them. The frequency shift (deflection signal in the tuning fork) is directly corrected from the tuning fork electrodes, while tunneling current is taken via the sample. Figures 3a,b compare STM and nc-AFM images obtained at the same area at 5 K. The AFM image was measured in the range of attractive tip−sample interaction, and the tip−sample distance was comparable to that used in the STM measurements above. While the Moiré pattern of the ZnO layer is clearly observed in the STM image (Figure 3a), the same ZnO layer is apparently flat in the AFM image (Figure 3b). This suggests that the ZnO layers are atomically flat and that the Moiré pattern results from the corrugation of the local density of state (LDOS)[25] due to the lattice mismatch between ZnO and Ag(111), rather than from a geometrical rippling of the ZnO layer.[24] In the AFM image (Figure 3b), some of the edge and corner of the ZnO islands have a pronounced contrast that is presumably related to a geometric strain. AFM also clearly shows a local defect in the island as indicated by the red dashed circle in Figure 3b, whereas this is rather difficult to see in the STM image (Figure 3a). Since the apparent height in STM is associated with the LDOS of surfaces, it is not necessarily identical to the geometrical height. Consequently, STM heights of ultrathin insulating films often show a bias-voltage dependence,[31,34−36] which complicates determining the real height for the film. On the other hand, the apparent height in AFM is dominated by weak chemical interactions (e.g., van der Waals force) between the surface and tip apex. Figure 3c shows the sample-bias voltage dependence of the STM apparent height of the low-ZnO (cyan circles) and high-ZnO (red circles) layers. Figure 3c also shows dI/dV spectra measured over the low-ZnO (cyan line) and high-ZnO (red line) layers. The onset of the spectrum at ∼1.8 (∼1.4) V for the low (high)-ZnO layer is assigned to the lower edge of the conduction band that contributes significantly to the increase of the apparent height. A similar behavior was reported for cobalt oxide films on Ag(001).[31] Figure 3d shows line profiles for the STM (black curve) and nc-AFM (gray curve) images, along the dashed white line in Figures 3a,b. In both cases, the apparent height is carefully calibrated by the monatomic step height of Ag(111) (2.36 Å). The nc-AFM heights of the low- and high-ZnO layers are 4.0 ± 0.3 and 6.1 ± 0.3 Å, respectively, which are approximately equal to those of STM at a bias voltage in the band gap region (e.g., 3.8 ± 0.3 and 5.8 ± 0.3 Å at V_s = 1 V).

dx.doi.org/10.1021/jp509013p | J. Phys. Chem. C 2014, 118, 27428−27435

For the first time, we also observed an atomic resolution AFM image of the ZnO(0001)-(7 × 7)/Ag(111)-(8 × 8) for the high-ZnO layer (Figure 4). The measured lattice constant

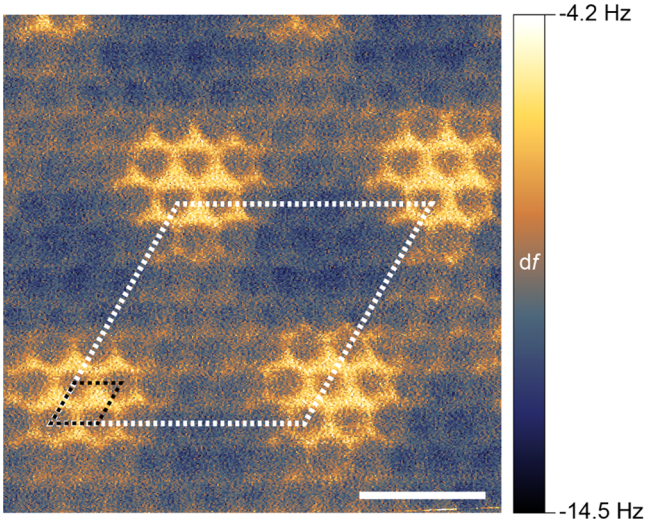

Figure 4. Atomic resolution AFM image of the high-ZnO layer on Ag(111) obtained with constant-height mode (V_s = 1 μV, A_{osc} = 0.3 nm, scale bar = 1 nm) at 5 K. The tip apex is modified by an unknown contaminant. The unit cells of the ZnO lattice (black dashed line) and Moiré pattern (white dashed line) are indicated.

of 3.3 ± 0.2 Å is in good agreement with $a_{ZnO,film}$ determined by the Moiré periodicity (Figure 2c). However, it should be noted that the tip apex was modified by an unknown contaminant, presumably a small molecule (the atomic resolution could not be obtained under usual tip conditions). It is known that the molecular tip causes a pronounced resolution in nc-AFM.[37] In addition, in Figure 4 the Moiré pattern is clearly observed, which is most probably due to the modified tip apex and considerably different force region from Figure 3b (that was measured with constant frequency shift of −1 Hz).

We did not observe a ZnO layer that is lower than the STM (AFM) apparent height of 3.8 (4.0) ± 0.3 Å at any coverage. This is much higher compared to those observed for a single ZnO layer on Pd(111)[12] (∼2.0 Å) and Pt(111)[26] (∼1.8 Å). On the other hand, the step height of ∼2 Å between the low- and high-layer is very consistent with that of 2.10 ± 0.1 Å determined for the coverage of 2.7 ML by SXRD measurement.[23] These results imply that the low-ZnO layer on Ag(111) corresponds to a bilayer. Therefore, we suggest that the low and high layer corresponds to the bi- and trilayer, respectively. The exclusive growth above 2 ML ZnO layers on Ag(111) is in line with the previous suggestion based on comparative AES studies of ZnO films on Pt(111) and Ag(111).[13] Additionally, it was found that the transition from the mono- to bilayer of ZnO films occurs on Pd(111) when the relatively high oxygen pressures (at least 5 × 10^{-6} mbar) was used during the reactive deposition.[26] Our condition (the oxygen pressure of 1 × 10^{-5} mbar) is consistent with this observation. On the other hand, we did not observe ordered ZnO layers at relatively low oxygen pressure. It is to be noted that the direct comparison of the physical height with the STM and AFM apparent height is not straightforward, especially for the boundary between different materials (ZnO and Ag in our case). This is because that the STM and AFM involves significant contributions from the electronic states (as shown in Figure 3c) and the force gradient acting between the tip apex and surface, respectively, which is different between the ZnO layers and Ag surface. In order to gain further insights, a comparison between accurate experimental data and high-level DFT calculations including SPM simulation (where tip contributions are incorporated) is required. In DFT calculations the interlayer distance between oxide films and metal surfaces is a key parameter relating to the issue. However, one has to examine carefully the exchange-correlation functionals to correct van der Waals contribution because the nonlocal dispersion energy considerably affects the interlayer distance of a metal/oxide interface.[38]

Finally, we demonstrate a feasible identification of the different ZnO layers based on their electronic structure. Figure 5 shows STS (dI/dV) maps (right) measured simultaneously

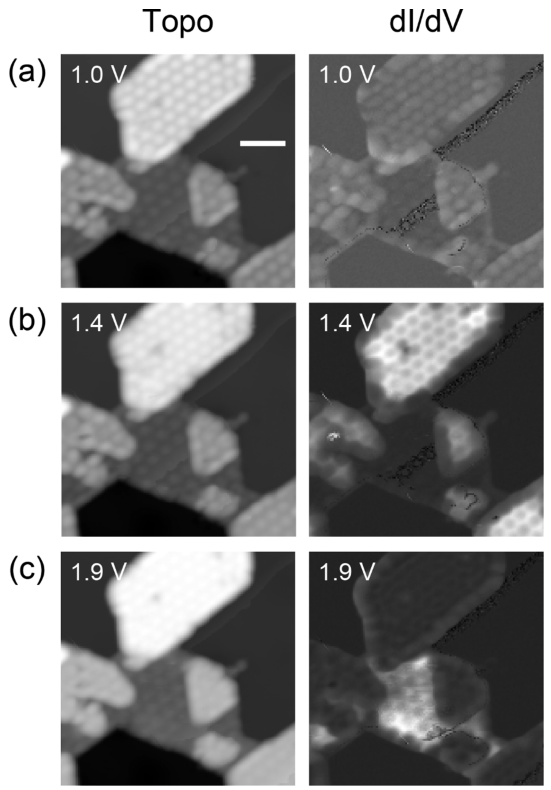

Figure 5. Simultaneous topographic images (left) and dI/dV maps (right) of ZnO layers on Ag(111) at 5 K with V_s = (a) 1.0, (b) 1.4, and (c) 1.9 V, I_t = 5 nA (scale bar = 5 nm). The bright (dark) fuzzy lines in the topo images (dI/dV maps) are probably ascribed to be mobile impurities.

with the topographic STM images (left). At lower bias (V_s = 1.0 V in Figure 5a), i.e., in the band gap region, both of the low- and high-ZnO layers are dark in the dI/dV map (off resonance). Since the high-ZnO layer has the onset of the resonance state around ∼1.4 eV (Figure 2c), the corresponding area becomes bright (on resonance) in the dI/dV map at V_s = 1.4 V compared to the low-ZnO state (Figure 5b). On the other hand, at V_s = 1.9 V the low-ZnO layer becomes bright (Figure 5c). Under the resonance conditions (Figures 5b,c), the Moiré protrusions in the STM images turn into depressions in the dI/dV maps, similar to observations for iron oxide films on Pt(111).[39,40] It also suggests that the Moiré pattern originates from the LDOS corrugation. Note that dI/dV intensities at the film edges and defects are noticeably weak in Figures 5b,c, indicating the modification of the local electronic states.[31,35,41]

dx.doi.org/10.1021/jp509013p | J. Phys. Chem. C 2014, 118, 27428−27435

CONCLUSIONS

We investigated the growth of ultrathin ZnO layers on Ag(111) prepared by the reactive deposition method. The local geometric and electronic structure was characterized using the simultaneous STM and nc-AFM measurement and STS at 5 K. The STM image of the ZnO layers shows a characteristic Moiré pattern resulting mainly from the LDOS corrugation due to the lattice mismatch between the ZnO layer and Ag(111) surface. However, the Moiré pattern was not observed in nc-AFM when measured at relatively large gap distances, indicating an atomically flat, nonbuckled structure of the ZnO layer as reported previously. For the first time, we also observed an atomic resolution nc-AFM image for ZnO(0001)-(7 × 7)/Ag(111)-(8 × 8) coincidence structure. The apparent height of STM strongly depends on the bias voltage, while it becomes comparable with that of nc-AFM when the bias voltage in STM is below the band gap of the ZnO layer. The ZnO layers with the STM (AFM) apparent height of 3.8 (4.0) ± 0.3 Å and 5.8 (6.1) ± 0.3 Å were observed. On the other hand, STS mapping of the resonance state of the ZnO layers allows us to discriminate the different layers. Our results suggest that ZnO layers on Ag(111) grow predominantly as bi- and trilayers under the conditions used.

ASSOCIATED CONTENT

Supporting Information

Large-scale STM images of several domains with slightly different azimuthal orientations and corresponding LEED patterns. This material is available free of charge via the Internet at http://pubs.acs.org.

AUTHOR INFORMATION

Corresponding Author

*Phone +49 (0)30 8413 5110; e-mail kuma@fhi-berlin.mpg.de (T.K.).

Notes

The authors declare no competing financial interest.

ACKNOWLEDGMENTS

We acknowledge financial support from the German Research Foundation (DFG) via the collaborative research center SFB 951 "Hybrid Inorganic/Organic Systems". A.S. acknowledges the support of the Japan Society for the Promotion of Science (JSPS). B.H.L. acknowledges support by the International Max-Planck Research School Functional Interfaces in Physics and Chemistry. T.K. acknowledges the support of Morino Foundation for Molecular Science.

REFERENCES

(1) Freund, H.-J.; Pacchioni, G. Oxide Ultra-thin Films on Metals: New Materials for the Design of Supported Metal Catalysts. *Chem. Soc. Rev.* **2008**, *37*, 2224−2242.

(2) Giordano, L.; Pacchioni, G. Oxide Films at the Nanoscale: New Structures, New Functions, and New Materials. *Acc. Chem. Res.* **2011**, *44*, 1244−1252.

(3) Shaikhutdinov, S.; Freund, H.-J. Ultrathin Oxide Films on Metal Supports: Structure-Reactivity Relations. *Annu. Rev. Phys. Chem.* **2012**, *63*, 619−633.

(4) Jaeger, R. M.; Kuhlenbeck, H.; Freund, H.-J.; Wuttig, M.; Hoffmann, W.; Franchy, R.; Ibach, H. Formation of a Well-ordered Alminium Oxide Overlayer by Oxidation of NiAl(110). *Surf. Sci.* **1991**, *259*, 235−252.

(5) Kresse, G.; Schmid, M.; Napetschnig, E.; Shishkin, M.; Köhler, L.; Varga, P. Structure of the Ultrathin Aluminum Oxide Film on NiAl(110). *Science* **2005**, *308*, 1440−1442.

(6) Biener, M. M.; Friend, C. M. Heteroepitaxial Growth of Novel MoO_3 Nanostructures on Au(111). *Surf. Sci.* **2004**, *559*, L173−L179.

(7) Deng, X.; Quek, S. Y.; Biener, M. M.; Biener, J.; Kang, D. H.; Schalek, R.; Kaxiras, E.; Friend, C. M. Selective Thermal Reduction of Single-Layer MoO_3 Nanostructures on Au(111). *Surf. Sci.* **2008**, *602*, 1166−1174.

(8) Nilius, N. Properties of Oxide Thin Films and Their Adsorption Behavior Studied by Scanning Tunneling Microscopy and Conductance Spectroscopy. *Surf. Sci. Rep.* **2009**, *64*, 595−659.

(9) Netzer, F. P.; Allegretti, F.; Surnev, S. Low-dimensional Oxide Nanostructures on Metals: Hybrid Systems with Novel Properties. *J. Vac. Sci. Technol., B* **2010**, *28*, 1−16.

(10) Sun, Y.-N.; Qin, Z.-H.; Lewandowski, M.; Carrasco, E.; Sterrer, M.; Shaikhutdinov, S.; Freund, H.-J. Monolayer Iron Oxide Film on Platinum Promotes Low Temperature CO Oxidation. *J. Catal.* **2009**, *266*, 359−368.

(11) Sun, Y.-N.; Giordano, L.; Goniakowski, J.; Lewandowski, M.; Qin, Z.-H.; Noguera, C.; Shaikhutdinov, S.; Pacchioni, G.; Freund, H.-J. The Interplay between Structure and CO Oxidation Catalysis on Metal-Supported Ultrathin Oxide Films. *Angew. Chem., Int. Ed.* **2010**, *49*, 4418−4421.

(12) Martynova, Y.; Liu, B.-H.; McBriarty, M. E.; Groot, I. M. N.; Bedzyk, M. J.; Shaikhutdinov, S.; Freund, H.-J. CO Oxidation over ZnO Films on Pt(111) at Near-atmospheric Pressures. *J. Catal.* **2013**, *301*, 227−232.

(13) Pan, Q.; Liu, B. H.; McBriarty, M. E.; Martynova, Y.; Groot, I. M. N.; Wang, S.; Bedzyk, M. J.; Shaikhutdinov, S.; Freund, H.-J. Reactivity of Ultra-Thin ZnO Films Supported by Ag(111) and Cu(111): A Comparison to ZnO/Pt(111). *Catal. Lett.* **2014**, *144*, 648−655.

(14) Ovesen, C. V.; Clausen, B. S.; Schiøtz, J.; Stoltze, P.; Topsøe, H.; Nørskov, J. K. Kinetic Implications of Dynamical Changes in Catalyst Morphology during Methanol Synthesis over Cu/ZnO Catalysts. *J. Catal.* **1997**, *168*, 133−142.

(15) Spencer, M. S. The Role of Zinc Oxide in Cu/ZnO Catalysts for Methanol Synthesis and the Water-Gas Shift Reaction. *Top. Catal.* **1999**, *8*, 259−266.

(16) Grunwaldt, J. D.; Molenbroek, A. M.; Topsoe, N. Y.; Toposoe, H.; Clausen, B. S. *In Situ* Investigations of Structural Changes in Cu/ZnO Catalysts. *J. Catal.* **2000**, *194*, 452−460.

(17) Ellmer, K., Klein, A., Rech, B., Eds.; *Transparent Conductive Zinc Oxide: Basics and Applications in Thin Film Solar Cells*; Springer Series in Materials Science 104; Springer: Berlin, 2008.

(18) Morkoç, H.; Özgür, U. *Zinc Oxide: Fundamentals, Materials and Device Technology*; Wiley-VCH: Weinheim, 2009.

(19) Shan, F. K.; Kim, B. I.; Liu, G. X.; Liu, Z. F.; Sohn, J. Y.; Lee, W. J.; Shin, B. C.; Yu, Y. S. Blue-shift of Near Band Edge Emission in Mg Doped ZnO Thin Films and Aging. *J. Appl. Phys.* **2004**, *95*, 4772−4776.

(20) Kourouklis, H. N.; Nix, R. M. The Growth and Structure of ZnO_x Overlayers on Low Index Silver Surfaces. *Surf. Sci.* **1994**, *318*, 104−114.

(21) Claeyssens, F.; Freeman, C. L.; Allan, N. L.; Sun, Y.; Ashfold, M. N. R.; Harding, J. H. Growth of ZnO Thin Films—Experiment and Theory. *J. Mater. Chem.* **2005**, *15*, 139−148.

(22) Freeman, C. L.; Claeyssens, F.; Allan, N. L.; Harding, J. H. Graphitic Nanofilms as Precursors to Wurtzite Films: Theory. *Phys. Rev. Lett.* **2006**, *96*, 066102.

(23) Tusche, C.; Meyerheim, H. L.; Kirschner, J. Observation of Depolarized ZnO(0001) Monolayers: Formation of Unreconstructed Planar Sheets. *Phys. Rev. Lett.* **2007**, *99*, 026102.

(24) Stavale, F.; Pascua, L.; Nilius, N.; Freund, H.-J. Morphology and Luminescence of ZnO Films Grown on a Au(111) Support. *J. Phys. Chem. C* **2013**, *117*, 10552−10557.

(25) Deng, X.; Yao, K.; Sun, K.; Li, W.-X.; Lee, J.; Matranga, C. Growth of Single- and Bilayer ZnO on Au(111) and Interaction with Copper. *J. Phys. Chem. C* **2013**, *117*, 11211−11218.
(26) Weirum, G.; Barcaro, G.; Fortunelli, A.; Weber, F.; Schennach, R.; Surnev, S.; Netzer, F. P. Growth and Surface Structure of Zinc Oxide Layers on a Pd(111) Surface. *J. Phys. Chem. C* **2010**, *114*, 15432−15439.
(27) Schott, V.; Oberhofer, H.; Birkner, A.; Xu, M.; Wang, Y.; Muhler, M.; Reuter, K.; Wöll, C. Chemical Activity of Thin Oxide Layers: Strong Interactions with the Support Yield a New Thin-Film Phase of ZnO. *Angew. Chem., Int. Ed.* **2013**, *52*, 11925−11929.
(28) Giessibl, F. J. High-Speed Force Sensor for Force Microscopy and Profilometry Utilizing a Quartz Tuning Fork. *Appl. Phys. Lett.* **1998**, *73*, 3956−3958.
(29) Giessibl, F. J. Atomic Resolution on Si(111)-(7 × 7) by Noncontact Atomic Force Microscopy with a Force Sensor Based on a Quartz Tuning Fork. *Appl. Phys. Lett.* **2000**, *76*, 1470−1472.
(30) Majzik, Z.; Setvín, M.; Bettac, A.; Feltz, A.; Cháb, V.; Jelínek, P. Simultaneous Current, Force and Dissipation Measurements on the Si(111) 7 × 7 Surface with an Optimized qPlus AFM/STM Technique. *Beilstein J. Nanotechnol.* **2012**, *3*, 249−259.
(31) Shantyr, R.; Hagendorf, Ch.; Neddermeyer, H. Scanning Tunneling Microscopy and Spectroscopy Studies on Structural and Electronic Properties of Thin Films of Co Oxides and Oxide Precursor States on Ag(001). *Thin Solid Films* **2004**, *464*, 65−75.
(32) Caffio, M.; Atrei, A.; Cortigiani, B.; Rovida, G. STM Study of the Nanostructures Prepared by Deposition of NiO on Ag(001). *J. Phys.: Condens. Matter* **2006**, *18*, 2379−2384.
(33) Rota, A.; Altieri, S.; Valeri, S. Growth of Oxide-Metal Interfaces by Atomic Oxygen: Monolayer of NiO(001) on Ag(001). *Phys. Rev. B* **2009**, *79*, 161401R.
(34) Joshi, S.; Ecija, D.; Koitz, R.; Iannuzzi, M.; Seitsonen, A. P.; Hutter, J.; Sachdev, H.; Vijayaraghavan, S.; Bischoff, F.; Seufert, K.; et al. Boron Nitride on Cu(111): An Electronically Corrugated Monolayer. *Nano Lett.* **2012**, *12*, 5821−5828.
(35) Sebastian, I.; Neddermeyer, H. Scanning Tunneling Microscopy on the Atomic and Electronic Structure of CoO Thin Films on Ag(100). *Surf. Sci.* **2000**, *454*−*456*, 771−777.
(36) Hansen, K. H.; Worren, T.; Lægsgaard, E.; Besenbacher, F.; Stensgaard, I. Bias Dependent Apparent Height of an Al_2O_3 Thin Film on NiAl(110), and of Supported Pd Clusters. *Surf. Sci.* **2001**, *475*, 96−102.
(37) Gross, L.; Mohn, F.; Moll, N.; Liljeroth, P.; Meyer, G. The Chemical Structure of a Molecule Resolved by Atomic Force Microscopy. *Science* **2009**, *325*, 1110−1114.
(38) Ling, S.; Watkins, M. B.; Shluger, A. L. Effects of Atomic Scale Roughness at Metal/Insulator Interface on Metal Work Function. *Phys. Chem. Chem. Phys.* **2013**, *15*, 19615−19624.
(39) Rienks, E. D. L.; Nilius, N.; Rust, H.-P.; Freund, H.-J. Surface Potential of a Polar Oxide Film: FeO on Pt(111). *Phys. Rev. B* **2005**, *71*, 241404R.
(40) Giordano, L.; Pacchioni, G.; Goniakowski, J.; Nilius, N.; Rienks, E. D. L.; Freund, H.-J. Interplay between Structural, Magnetic, and Electronic Properties in a FeO/Pt(111) Ultrathin Film. *Phys. Rev. B* **2007**, *76*, 075416.
(41) Simic-Milosevic, V.; Nilius, N.; Rust, H.-P.; Freund, H.-J. Local Band Gap Modulations in Non-stoichiometric V_2O_3 Films Probed by Scanning Tunneling Spectroscopy. *Phys. Rev. B* **2008**, *77*, 125112.